# Influence of Concrete Carbonation on Electromagnetic Permittivity Measured by GPR and Capacitive Techniques

Xavier Derobert, Géraldine Villain, Jean-Paul Balayssac

# INFLUENCE OF CONCRETE CARBONATION ON ELECTROMAGNETIC PERMITTIVITY MEASURED BY GPR AND CAPACITIVE TECHNIQUES

Dérobert X.[1], Villain G.[1], Balayssac J.P.[2]

[1]IFSTTAR, CS5004, F-44344 Bouguenais cedex, France

Email: xavier.derobert@ifsttar.fr

[2]LMDC, INSA/UPS Génie Civil, F-31077 Toulouse cedex 04, France

## ABSTRACT

This paper addresses the effect of concrete carbonation on the propagation and dispersion of electromagnetic (EM) waves and the capability of two electromagnetic non-destructive techniques to detect this pathology. A capacitive technique operating at low frequency (around 33 MHz) and a ground penetrating radar (GPR - called the 1.5-GHz antenna) are tested for the monitoring of reinforced concrete structures. To better understand the phenomena involved in concrete carbonation, the results of two complementary experimental campaigns are analyzed for saturated concretes. First, the dispersion curves of complex permittivity are measured for both carbonated and non-carbonated samples by a cylindrical coaxial EM cell. Due to carbonation, the permittivity decreases and the level of dispersion reduces slightly. Second, using GPR (coupled at approx. 900 MHz) and capacitive measurements conducted on controlled slabs, it is confirmed that the real part of the relative permittivity decreases within a range of 2 at 33 MHz and a range of 1 toward 900 MHz, while the radar signal amplitude increases.

## 1. Introduction

The diagnosis of concrete structures has become a major issue over time. Among the main durability indicators, salt ingress and carbonation constitute the major causes in most deterioration processes, facilitated by water content as a common agent, thus leading to rebar corrosion. Electromagnetic (EM) non-destructive testing (NDT) techniques have, through numerous studies, revealed their sensitivity and efficiency in evaluating such durability indicators. These studies have mainly been devoted to water content evaluation or chloride ingress monitoring in concrete [Robert, 1998; Soustos *et al.*, 2001; Laurens *et al.*, 2002; Peer *et al.*, 2003; Hugenschmidt and Loser, 2008; Dérobert *et al.*, 2008; Kalogeropoulos *et al.*, 2013; Villain *et al.*, 2015; Hong *et al.*, 2017; Dérobert and Villain, 2017a], but little emphasis has been paid to carbonation [Hong *et al.*, 2017; Balayssac *et al.*, 2012; Dérobert and Villain, 2017b].

Carbonation is a major contributor to concrete degradation. Due to climate change, carbon dioxide ($CO_2$) content has been drastically increasing in the atmosphere, reaching above 400 ppm in the world and in 2016 extending to the less polluted parts of the Indian Ocean [Ballantyne *et al.*, 2012; Ramonet *et al.*, 2016]. In urban areas, the mean value is even higher. Moreover, due to human activity, daily variations are

Preprint
*Journal of Environmental and Engineering Geophysics* (2018), 23 (4)
http://dx.doi.org/10.2113/JEEG23.4.443

considerably higher in suburban areas than in rural zones; for example, in suburban London and coastal Ireland, variation factors of 72 can be found [Hernández-Paniagua *et al.*, 2015]. Concrete structures are therefore slightly more affected by carbonation [De Larrard *et al.*, 2014]. The acidification in cover concrete leads to severely corrosive pathologies of reinforced concrete structures [Tuutti, 1982; Parrott, 1987; Dunster, 1989; Papadakis *et al.*, 1991a-b; Villain and Platret, 2006; Villain and Thiéry, 2005].

In light of this context and given that the wave propagation of EM NDT techniques is sensitive to both porosity and chemical changes in concrete material, such techniques can become useful tools in estimating the carbonation level of cover concrete. The aim of this paper is to study the effect of carbonation on the propagation and dispersion of EM waves at low and higher radar frequencies in order to make use of the capacitive technique and GPR during inspections of reinforced concrete structures. A previous study [Dérobert and Villain, 2017b] found a negligible effect of carbonation on dry concrete mix, hence the present paper is focused on saturated mixes.

After an overview of the concrete carbonation process and its consequences provided in the next section, the experimental programs of two complementary research projects [Balayssac *et al.*, 2012; Dérobert and Villain, 2017b] are presented, including their concrete mixes, conditioning and the EM NDT techniques employed. The final section is devoted to reporting results and discussing their analysis.

## 2. The concrete carbonation process

One of the main causes of corrosion in reinforced concrete structures is carbonation, a phenomenon due to the penetration of carbon dioxide into cover concrete [Tuutti, 1982; Parrott, 1987]. The carbonation process leads to physicochemical changes in the cover concrete, which can be detailed as follows.

### 2.1 Carbonation process

The reinforcing bars in reinforced concrete structures are physically and chemically protected from corrosion by the concrete. From a chemical point of view, the very high pH-value of concrete (around 12.6) leads to a passivation of the reinforcement. Over time, atmospheric carbon dioxide ($CO_2$) can penetrate into concrete, dissolve in the pore solution and react with portlandite ($Ca(OH)_2$), as illustrated by Equation (1) or with C-S-H according to Equation (2):

$$Ca(OH)_2 + CO_2 \rightarrow CaCO_3 + H_2O \quad (1)$$

$$C\text{-}S\text{-}H + CO_2 \rightarrow CaCO_3 + H_2O + \text{silica gels} \quad (2)$$

These effects result in water formation, the precipitation of calcium carbonates ($CaCO_3$) and amorphous silica gels [Dunster, 1989]. The equilibrium between portlandite, C-S-H and the hydroxide ions of the pore solution is thus changed, leading to the gradual consumption of all reserve basicity and then to a drop in pH-value from about 13 to 9. The reinforcement is no longer chemically protected and more likely to corrode.

According to numerous studies [Tuutti, 1982; Parrott, 1987; Dunster, 1989; Papadakis *et al.*, 1991a-b; Villain and Thiéry, 2005; Villain and Platret, 2006], carbonated depth increases with the square root of time

following a simplified Fick's diffusion law. The parameters of this law depend on many factors, including concrete mix design, especially the water-cement ratio, and fabrication and environmental exposure conditions. Among existing carbonation models, Papadakis *et al.* [1991a-b] were able to determine the depth of carbonation and induced mass changes in the various mix components; their work encompassed the cement chemical analysis and external conditions detailed in Section 3.

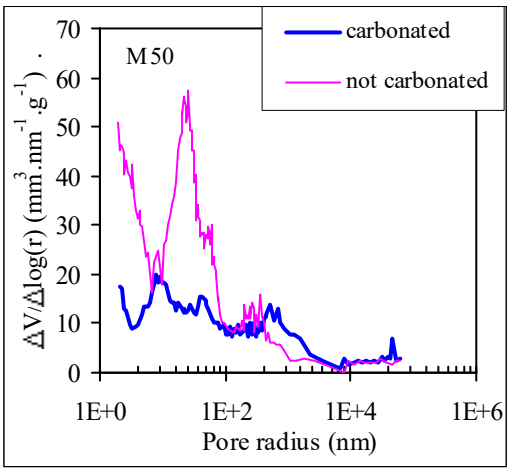


Fig. 1: Example of pore size distribution in both carbonated and non-carbonated concrete [Villain and Platret, 2006].

## 2.2 Consequences on physical properties

The carbonation of concrete induces several consequences. The first is a reduction in porosity due to $CaCO_3$ precipitation and the formation of amorphous silica gels filling the small pores [Parrott, 1987; Dunster, 1989; Villain and Thiéry, 2005; Glass *et al.*, 1991], as shown in Figure 1. The order of magnitude of this porosity reduction lies between 2% and 4% for two concretes mixed with Portland cement (namely M25 and M50), with a mean compressive strength of 25 MPa and 50 MPa at 28 days, according to Villain and Thiéry [2005].

The other major consequences are: the release of liquid water that can locally change the water content (hence the preference for conducting comparative measurements under saturated conditions); the pH-value decrease from roughly 13 to 9; and carbonation-induced change in the ionic content of the pore solution.

Three indirect and secondary consequences can be cited. First, let's observe the increase in mechanical strength [Parrott, 1987]. Second, carbonation induces a change in both permeability and the diffusion coefficient. These transport coefficients often decrease following a drop in porosity; conversely, an increase can be noted for very porous concretes, witnessed as a larger pore appearance and a tortuosity reduction [Villain and Thiéry, 2005]. Third and last, the resistivity of concrete, which increases with carbonation, is attributed to a loss of porosity and the disappearance of mobile ions ($OH^-$) from the pore solution [Alonso *et al.*, 1988; Glass *et al.*, 1991]. The ratio of resistivities measured on saturated carbonated (*C*) and non-carbonated *(NC)* specimens equals between 1.8 and 8 for M25 to M50 concretes mixed with Portland cement [Villain and Thiéry, 2005].

Various experimental methods can be performed to evaluate concrete carbonation. The best known and

easiest to use is a pH-indicator, like phenolphthalein, sprayed onto a freshly broken surface sample. This method allows defining a depth of carbonation $P_c$ correlated with the pore solution pH-value [AFPC-AFREM, 1997]. Another method, based on $CO_2$ fixation, entails tracking the mass increase by weighing. The weakness of this method lies in the fact that weight can be biased by moisture change, e.g. concomitant drying due to accelerated carbonation taking place in a chamber with relative humidity (RH) controlled at around 50%. For both non- and fully-carbonated specimens, the bulk porosity reduction can be measured by water saturation under vacuum [AFPC-AFREM, 1997].

## 3. Experimental campaigns

The results presented herein stem from two complementary research programs sponsored respectively by the French Ministry of Ecology (MTES) and EDF company (electric utility), and the French National Research Agency (ANR). The first program, called Epsilon, seeks to quantify, through several large experimental designs [Dérobert and Villain, 2017a-b], the influence of composition parameters and concrete conditions on permittivity within a frequency band of approx. [50 MHz - 1 GHz]. The second program, ANR-SENSO, was devoted to evaluating durability indicators (namely porosity and carbonation depth) by applying various types of NDT methods [Balayssac *et al.*, 2012] on several controlled homogeneous mixes in the laboratory. Since the aggregate and cement contents were identical, these common components offer the possibility of collating results for the two projects.

### 3.1 Concrete mix design from the Epsilon project

The mix design used for the Epsilon experimental program is presented in Table 1, which lists 12 concretes submitted to carbonation. The codes employed to design these concrete mixes are kept similar to the original ones (C1 to C31), as presented in [Dérobert and Villain, 2017b], in order to facilitate subsequent studies by readers. The effective water-cement ratio (W/C) ranges from 0.35 to 0.55, resulting in a porosity varying from 6.7% to 17.1%. Standard Portland cement CEM I 42.5 R (Heidelberg Group) has been used, and the aggregates originating in the Nantes (FR) region are either calcareous (Boulonnais) or siliceous (Palvadeau).

**Table 1: Concrete mix design and average porosity (Epsilon project)**

| Code | Aggregate type | Gravel 4/20 (kg/m$^3$) | Sand 0/4 (kg/m$^3$) | CEM I (kg/m$^3$) | W/C (-) | AEA* Fosroc | Poro. (%) |
|---|---|---|---|---|---|---|---|
| C1 | Calcareous | 1008 | 1008 | 350 | 0.35 | - | 13.7 |
| C3 | Siliceous | 932 | 932 | 410 | 0.35 | - | 8.9 |
| C5 | Siliceous | 985 | 985 | 350 | 0.35 | Yes | 6.7 |
| C7 | Calcareous | 953 | 953 | 410 | 0.35 | Yes | 10.8 |
| C13 | Siliceous | 917 | 917 | 350 | 0.5 | - | 10.8 |

| | | | | | | | |
|---|---|---|---|---|---|---|---|
| C15 | Calcareous | 872 | 872 | 40 | 0.5 | - | 14.6 |
| C17 | Calcareous | 939 | 939 | 350 | 0.5 | Yes | 15.5 |
| C19 | Siliceous | 853 | 853 | 410 | 0.5 | Yes | 16.9 |
| C25 | Calcareous | 916 | 916 | 350 | 0.55 | - | 13.5 |
| C27 | Siliceous | 826 | 826 | 410 | 0.55 | - | 13.6 |
| C29 | Siliceous | 894 | 894 | 350 | 0.55 | Yes | 17.1 |
| C31 | Calcareous | 845 | 845 | 410 | 0.55 | Yes | 14.9 |

*Air-entraining agent (AEA)

Three cylindrical samples (⌀75 x 70 mm) per test concrete were cored and 3 slabs (230 x 230 x 70 mm) sawn. Additional non-carbonated (*NC*) samples enabled determining the porosity. One core was preserved from carbonation (sample A) per concrete. Another core (sample B) was dried in an oven in order to reach a constant mass corresponding to an equilibrium at RH = 50%. Similarly, for each mix, 3 slabs (~22 × 22 × 6 cm) were sawn for capacitive measurements.

All the B samples and slabs were then placed in a chamber at approx. T = 20°C, RH = 50% and [$CO_2$] = 50% for 3 months, with samples being weighed once a month. The mass increased substantially during the first 2 months, while the last month tapered off or stabilized. The relative mass increase measured and calculated between times t0 and t0 + 3 months, as well as the predicted mean values and variation ranges using Papadakis' model, are summarized in Table 2: the values remain similar, with the measured values being slightly lower. For each concrete, porosity was measured by means of water saturation on one core per state.

**Table 2: Comparison of relative mass increases due to carbonation: estimated values by Papadakis' model with measured and calculated values after 3 months of accelerated carbonation (color legend: dark-medium-light gray and white as high, middle, low and very low levels of uncertainty, respectively).**

| Code | Relative mass increase (%) | | |
|---|---|---|---|
| | Estimated | Slabs | Cylinders |
| C1 | 4.±0.1 | 4.5 | 3.7 |
| C3 | 4.8±0.1 | 3.2 | 2.9 |
| C5 | 4.2±0.1 | 2.6 | 3.1 |
| C7 | 4.6±0.3 | 4.4 | 3.7 |
| C13 | 4.6±0.3 | 4.9 | 4.2 |
| C15 | 5.4±0.4 | 5.8 | 5.3 |
| C17 | 4.6±0.4 | 4.7 | 3.2 |
| C19 | 5.6±0.3 | 4.5 | 3.5 |
| C25 | 4.6±0.3 | 5.3 | 4.2 |
| C27 | 5.6±0.3 | 5.6 | 4.7 |
| C29 | 4.8±0.5 | 3.3 | 2.4 |
| C31 | 5.4±0.6 | 4.7 | 3.7 |

| Color code | ⌀Increase/Estimated (-) |
|---|---|
| | [-0.4, -0.55] |
| | [-0.2, -0.4[ |
| | [+0.2, -0.2[ |

For low-porosity concretes (C3 and C5), the measured values are less than the estimated values of relative mass increases. This result can be attributed to incomplete carbonation. For very porous concretes (C19 and C29), the samples should be completely carbonated; meanwhile, these carbonated samples were stored in the carbonated chamber at RH = 50% and thus could have been subjected to drying concomitant to carbonation. Furthermore, for all concretes mixed with an air-entraining agent (C5 and C7, C17 and C19, C29 and C31), porosity is high and may lead to overestimating the mass increase with Papadakis' model, which could provide a second plausible explanation of the differences observed in Table 2 for porous concretes C19 and C29.

Once the carbonation process had been performed, samples A and B were saturated under vacuum and tested in the cylindrical coaxial EM cell.

### 3.1 Concrete mix design from the ANR-SENSO project

The mix design used for the ANR-SENSO experimental program, in which only 5 concretes were subjected to carbonation, is presented in Table 3. Two additional slabs, cured just like the others, were cored in order to characterize the concretes [Balayssac *et al.*, 2012]. For each design, porosity was measured by means of water saturation on four cores from the first additional slab. The mean value and standard deviation are given in Table 3. The effective water-cement ratio ranges from 0.57 to 0.9, thus inducing a porosity from 14.9% to 18.1%.

Similarly to the Epsilon project, Portland cement CEM I and aggregates, either calcareous or siliceous, were used. Combining both projects extends the water-cement ratio from 0.35 to 0.9, corresponding to a range of porosity from 6.7% to 18.1%.

**Table 3: Concrete mix design and average porosity (ANR-SENSO project)**

| Code | Aggregate type | Gravel 4/14 (kg/m$^3$) | Sand 0/4 (kg/m$^3$) | CEM I (kg/m$^3$) | Water (kg/m$^3$) | W/C (-) | Poro. (%) |
|---|---|---|---|---|---|---|---|
| G3 | Siliceous | 1069 | 774 | 370 | 211.6 | 0.57 | 15.5±0.5 |
| G3a | Siliceous | 1069 | 774 | 370 | 211.6 | 0.57 | 16.0±0.7 |
| G7 | Siliceous | 1047 | 839 | 320 | 216.32 | 0.68 | 15.9±0.8 |
| G8 | Siliceous | 1016 | 938 | 240 | 217.2 | 0.9 | 18.1±1.0 |
| G6 | Calcareous | 1138 | 758 | 370 | 214 | 0.58 | 14.9±0.4 |

A total of 9 slabs (50 x 25 x 12 cm) were cast per test concrete. After a campaign devoted to studying water content [Dérobert and Villain, 2017b], 4 slabs per concrete were dried in an oven in order to reach a constant mass, corresponding to an equilibrium at RH = 50%, and then wrapped to homogenize water content inside the slabs. They were then subjected to accelerated carbonation under controlled conditions at about T =

20°C, RH = 50% and [$CO_2$] = 50% until the corresponding small sample had reached the required carbonation depth Pc at around 10, 20, 40 and 60 mm. The accelerated carbonation was verified by carbonation depth measurements conducted on additional samples (Table 4). For this step, several cores (from the 2nd additional slab) were subjected to the same curing, preconditioning and accelerated carbonation conditions. For each concrete, a core was split and sprayed with a phenolphthalein solution at different test times in order to determine carbonation depth according to the RILEM procedure "TC56-MHM Hydrocarbon materials, CPC-18 Measurement of hardened concrete carbonated depth". Once the targeted carbonation depth had been reached on this reference core, two carbonated slabs of the same concrete were removed from the carbonation chamber and carefully protected until the non-destructive test.
Parameters P0, P40 and P60, appended to the codes in Table 4, correspond to the following carbonation depth target values: 0, 40, and 60 mm, respectively.

**Table 4: Carbonation depths and porosity decreases**

| Code | Targeted Pc (mm) | Porosity (%) | Poro. difference (%) | Measured Pc (mm) |
|---|---|---|---|---|
| G3-Pc0 | 0 | 16.2 | 2.8 | 1 |
| G3-Pc40 | 40 | 13.4 | | 31 |
| G3a-Pc0 | 0 | 15 | 2.6 | 1 |
| G3a-Pc40 | 40 | 12.4 | | 29 |
| G7-Pc0 | 0 | 15.8 | 1.6 | 3 |
| G7-Pc40 | 40 | 14.2 | | 42 |
| G8-Pc0 | 0 | 18.1 | 2.8 | 5 |
| G8-Pc60 | 60 | 15.3 | | 60 |
| G6-Pc0 | 0 | 17.2 | 4.5 | 2 |
| G6-Pc40 | 40 | 12.7 | | 27 |

Note the extreme difficulty in reaching Pc = 40 mm, as the actual value in most cases was closer to 30 mm. Moreover, the decrease in porosity is slightly too small for G7~~, perhaps because a too high porosity of the non-carbonated (NC) sample that should be around 15% (Table 3)~~. In fact, except for G8, it proved to be very difficult, or even impossible, to reach complete carbonation corresponding to Pc = 60 mm (on both faces) after several months in the carbonation chamber. All slabs were then saturated and tested using different NDT methods, in particular capacitive and GPR techniques (as described in the following section).

## 3.2 NDT methods

Within the framework of this study, two EM NDT techniques were used (i.e. capacitive technique and GPR), complemented by measurements in an EM cell. All 3 techniques and methodologies will be described below.

### *3.2.1 GPR technique*

The radar technique employed relied on a commercial GPR system, using SIR-3000 systems from Geophysical Survey Systems, Inc. (GSSI®) and two separate ground-coupled 1.5-GHz antennas. GPR relies on the principle that electromagnetic wave pulses are transmitted through the investigated medium. As the EM signal passes through this medium, partial reflections occur at each interface, thus presenting EM contrasts that can be acquired as time signals by the receiving antenna. The recent literature detailing this technique includes Jol [2009], Pajewski and Benedetto [2011], Persico [2014] and Utsi [2017]. As regards concrete, the signals received are mainly analyzed in terms of time delay and pulse echo amplitude [Laurens, *et al.*, 2002; Dérobert *et al.*, 2008].

The GPR methodology proposed herein focuses on the direct wave in the medium recorded by the bistatic antennas using four offsets (transmitter-receiver distance) ranging from 7 to 14 cm, which in most instances are compatible with rebar mesh sizes. For our purposes, a commercial bistatic antenna was adapted to variable offsets while separating the shielded antennas and retaining the electronics and their connection (Fig. 2). An absorbent foam was placed between the transmitter and receiver during static measurements in order to measure the wave without distortion due to the direct air wave [Villain *et al.*, 2012]. All measurements were performed in air as the initial step, and subsequently on the concrete at three measurement points for each offset (Fig. 3a). After peaking the maximum direct wave (DW) for every offset, the velocity and relative permittivity can then be calculated (Fig. 3b). Since the antennas are coupled to the surveyed medium, the central frequency decreases towards approx. 900 MHz on saturated concretes, which is why results derived from GPR will be associated with the 900-MHz frequency in the following.

Few observables are studied with this configuration, i.e.: velocity, the corresponding relative permittivity, and attenuation from the direct wave. For this attenuation, the studied observable corresponds to the slope coefficient of the logarithm of normalized amplitudes of the four offsets (herein called amplitude-slope): the greater the slope, the less electromagnetically attenuating the medium.

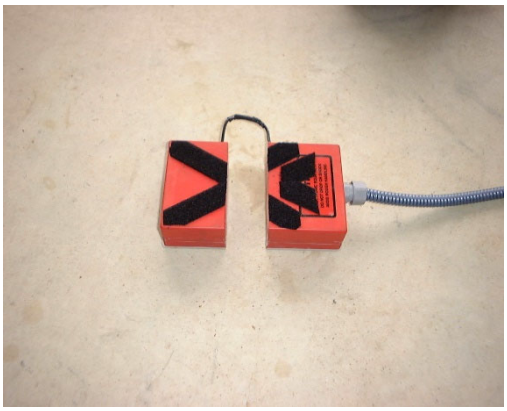

Fig. 2: Adaptation of a variable-offset bistatic configuration from one commercial 1.5-GHz antenna

a) b)

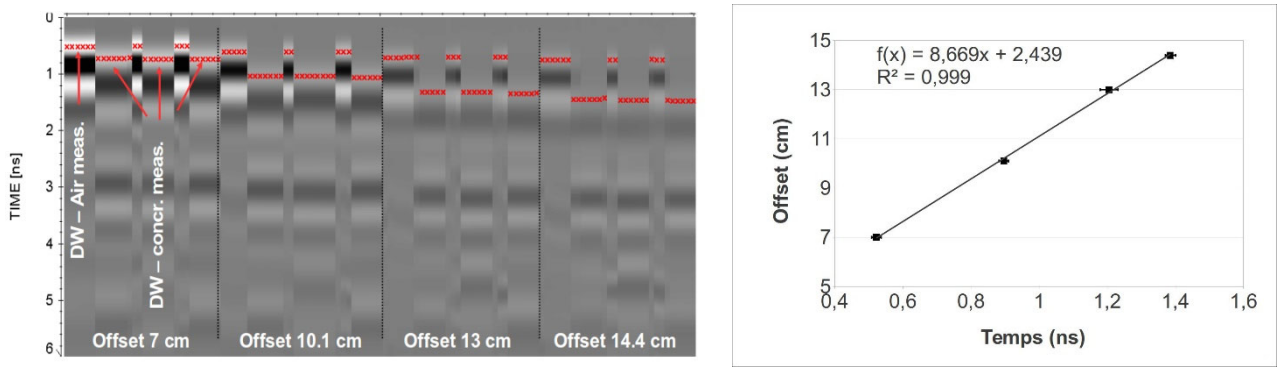


Fig. 3a) Example of GPR CMP performed on concrete G3 before carbonation - Presentation of the direct waves (DW) from air and concrete measurements at three positions; b) Calculation of GPR velocity from the peaking data

### *3.2.2 Capacitive technique*

The principle of the capacitive technique relies on the resonance frequency measurement of an oscillating circuit (approx. 33 MHz) between electrodes lying on the upper face of the test plane medium [Dérobert *et al.*, 2008; Fares *et al.*, 2016]. This set-up forms a coplanar capacitor. The changes in capacitance, which induce a shift in resonance frequency, are indicative of concrete constituents and conditions. A preliminary calibration on known materials outputs the relative permittivity of the tested material, which is viewed as a homogeneous medium. A panel of three sets of electrodes (investigation depth equal to 2-3 mm for electrodes labeled SE, 1-2 cm for ME, 7-8 cm for GE) yields information on a possible gradient depth function (Fig. 4).

For the present study, only those results obtained with the GE electrodes are shown. The thickness coupled with a set of electrodes, most closely resembling that from the GPR direct wave, actually corresponds to GE electrodes. Moreover, since a thin superficial layer was carbonated on ANR-SENSO slabs during NDT measurements (1 to 2 mm), the GE electrodes were least sensitive to this layer, leading to the assumption that its effect was negligible.

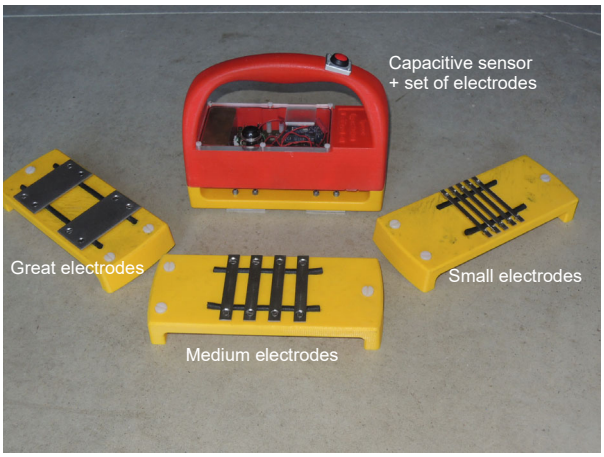


Fig. 4: Capacitive measurement system with 3 different sets of electrodes (SE, ME, GE)

### *3.2.3 Coaxial cylindrical EM cell*

An EM cell measurement was designed to characterize bound civil engineering materials, i.e. cement as well as bituminous concrete, through complex relative permittivity at radar frequencies typically extending from 50 MHz to about 1-1.4 GHz, with the upper limit depending on material permittivity. An iterative inversion

249 procedure enabled retrieving the complex relative permittivity of the material from the reflection coefficient
250 measurements [Adous *et al.*, 2006], thus deriving the dispersion curve (relative permittivity vs. frequency).
251 The benefit of such an EM cell is twofold: to characterize civil engineering mixes over a large radar
252 frequency band; and to correlate the measurements conducted by the two NDT techniques, namely capacitive
253 and GPR, operating at both ends of this frequency band. In order to extrapolate the relative permittivity at
254 33 MHz (or 1 GHz) from EM cell measurements and compare all results with those of the NDT technique, a
255 Jonscher's model was then introduced to fit the dispersion curve [Ihamouten *et al.*, 2011].
256

## 4. Results and analysis

### 4.1 Effect of carbonation on the complex relative permittivity

The NC cores (A) and carbonated cores (B) from Table 1 were tested in the EM coaxial cell under saturated conditions. The dispersion curve of the complex relative permittivity was obtained with an averaged higher frequency, depending on the value of the real part of permittivity (dielectric constant), limited at between approx. 750 MHz and 1 GHz. An example for concretes mixed with calcareous aggregates (C15) is given in Figure 5 and another with siliceous aggregates (C27) in Figure 6. As is the case for all concretes (except C3 and C29, which were not sufficiently carbonated, see Table 2), the complex permittivity decreases significantly with carbonation, especially at low frequency for the real part. Moreover, the carbonated saturated samples are less dispersive than the other samples.

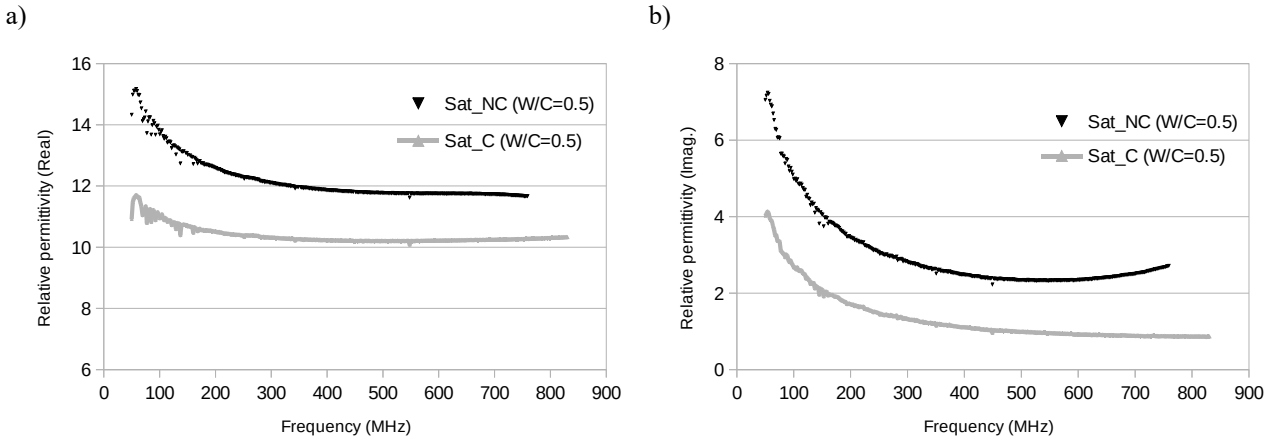


Fig. 5: Complex permittivity of carbonated (C) and non-carbonated (NC) saturated concrete C15 (calcareous aggregates, cement 410 kg.m$^{-3}$ and W/C = 0.5): a) Real part; b) Imaginary part

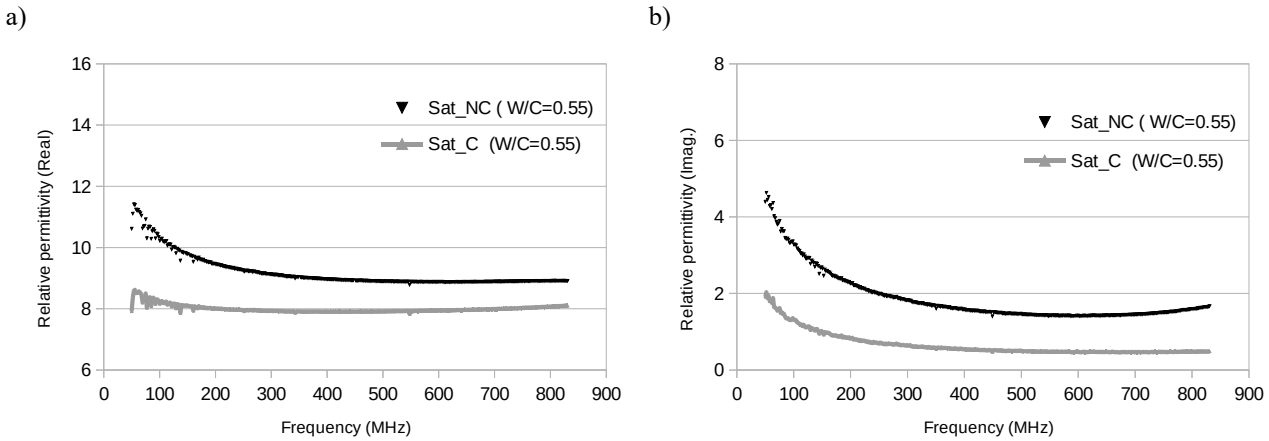


Fig. 6: Complex permittivity of carbonated (C) and non-carbonated (NC) saturated concrete C27 (siliceous aggregates, cement 410 kg.m$^{-3}$ and W/C = 0.55): a) Real part; b) Imaginary part

This decrease in permittivity may be due to the porosity reduction, estimated at approx. 4% (absolute value) for ordinary concretes by Villain *et al.* [2007], which induces an overall decrease in the pore solution of saturated samples. The diminished dispersive effects at low frequency (below 200 MHz) might also be due to

the decrease in small mobile hydroxyl ions ($OH^-$). Another explanation could be the filling of smaller pores (Fig. 1) combined with less tortuosity, which induces a reduction in the capacitive effects of the various ions contained in these pores.

Note that these explanation are similar to those given for the increase in resistivity induced by carbonation [Alonso *et al.*, 1988; Glass *et al.*, 1991].

The second observation focuses on the dispersive effects of permittivity at low frequency, which increase due to the Maxwell-Wagner effect as the W/C ratio decreases, as explained by the lower pore diameters.

Let's also note the carbonation of high performance concretes, with such a low W/C ratio and hence low porosity, is a very long and difficult process. Despite 3 months of exposure to a high carbon dioxide content, the carbonation process might still be incomplete for less porous concretes. A model based on a Portland cement quantity and W/C established by Papadakis *et al.* [1991a-b] found that the mass increase of a complete carbonation process is bound to be slightly overestimated, with the less porous concretes not being fully carbonated (dark and medium gray in Table 4).

Concerning concretes C3 and C29, ~~there must be an experimental problem, as C29 is a highly porous concrete (φ 1⁄4 17.1%) that should carbonate easily. This lack of carbonation may be due to the air-entraining agent that induces a closed porosity, but this is merely a hypothesis although noted on the other mixes containing AEA.~~ even though permittivity results show similar trends to those of C15 and C27, with slight decreases in permittivity, they should not be taken into account and are thus not presented herein.

Lastly, the difference in permittivity observed between NC samples of concretes mixed with calcareous and siliceous aggregates is solely due to the permittivity of the coarse aggregates.

### 4.2 Effect of carbonation on EM NDT techniques

The primary results from the ANR-SENSO project are listed in Table 5, with all mixes being considered homogeneous. The mean value and standard deviation correspond to several measurements performed at 3 points on the surface of the same slab. First, it can be underscored that the real part of the relative permittivity (or dielectric constant) is lower for carbonated slabs than for NC slabs, at low frequency for capacitive measurements as well as at higher frequencies for GPR measurements (though to a much lesser extent). This decrease is attributed to a drop in porosity, thus leading to less volumetric water content in the mixes.

A special comment is warranted for concrete G6, since its aggregates are of a different type. Calcareous coarse aggregates do involve mostly higher permittivity values, as G6 behaves like the other mixes under a carbonation process from an EM standpoint. For GPR, the measurement conducted on the G6_NC slab seems to be compromised and has thus been excluded.

**Table 5: Variation in permittivity (GPR and capacitive) and radar amplitude-slope due to carbonation (ANR-SENSO project)**

| Code | Porosity (%) | Capa_GE permittivity (-) | GPR permittivity (-) | GPR amplitude-slope (-) |
|---|---|---|---|---|
| G3-P0 | 16.2 | 15.4 ± 0.6 | 10.3 ± 1.3 | 0.34 ± 0.04 |
| G3-P40 | 13.4 | 12.4 ± 0.1 | 9.7 ± 0.3 | 0.50 ± 0.03 |
| G3a-P0 | 15 | 14.5 ± 0.1 | 12.0 ± 0.7 | 0.47± 0.03 |
| G3a-P40 | 12.4 | 11.6 ± 0.2 | 9.7 ± 0.1 | 0.52 ± 0.01 |
| G7-P0 | 15.8 | 15.5 ± 0.1 | 11.7 ± 0.7 | 0.44 ± 0.01 |
| G7-P40 | 14.2 | 12.9 ± 0.1 | 10.6 ± 0.6 | 0.47 ± 0.02 |
| G8-P0 | 18.1 | 15.2 ± 0.1 | 12.4 ± 0.5 | 0.38 ± 0.02 |
| G8-P60 | 15.3 | 13.0 ± 0.2 | 11.8 ± 0.6 | 0.49 ± 0.02 |
| G6-P0 | 17.2 | 16.5 ± 0.1 | 11.5 ± 0.5 | 0.39 ± 0.01 |
| G6-P40 | 12.7 | 14.0 ± 0.1 | 11.7 ± 0.4 | 0.42 ± 0.01 |

The increase in the radar amplitude-slope of the direct wave (Fig. 7b), in the carbonated material, deserves to be highlighted; it is correlated with the decrease in wave attenuation, hence with the decrease in the imaginary part of the relative permittivity, due to less volumetric water quantity in the saturated concretes. In assuming two outliers, the GPR amplitude-slope and relative permittivity show linear sensitivities to porosity (Fig. 7b). However, the lower level of uncertainty of the amplitude-slope leads to considering this observable as more efficient for carbonation detection.

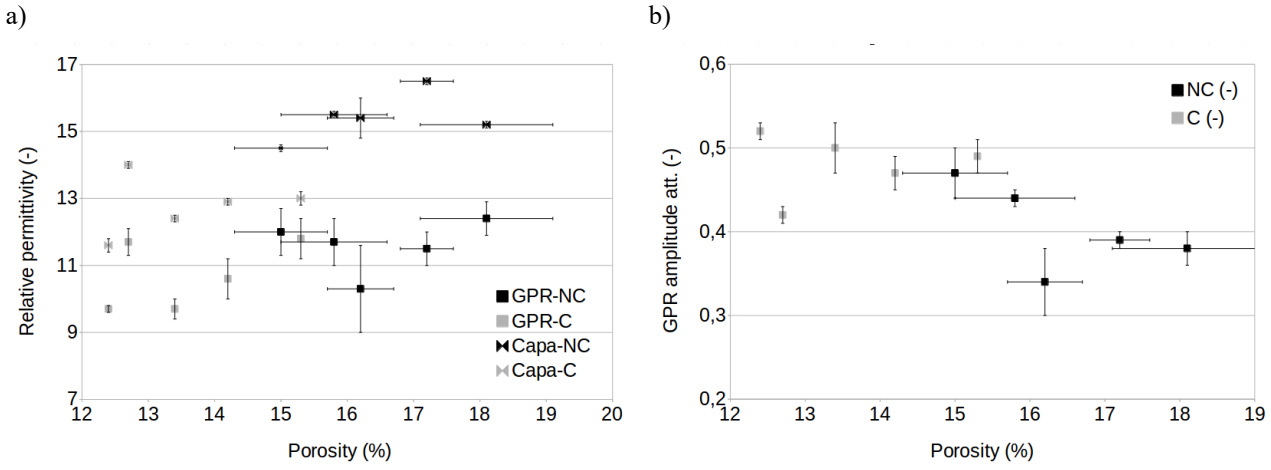


Fig. 7: a) GPR relative permittivity and (b) GPR amplitude-slope vs. porosity for carbonated and non-carbonated concrete mixes (ANR-SENSO project)

NDT techniques could be performed during the carbonation process as the carbonation depth could be measured. Figure 8 presents the evolution in relative permittivity vs. carbonation depth measured by both capacitive and GPR techniques on all mixes. We can detect a decreasing slope over the first 20 millimeters until reaching a plateau, which is clearly visible in Figure 8a for capacitive measurements. This finding can be interpreted as an increase in the share of carbonation thickness within the volume coupled to the GE

electrodes (assimilated to a depth penetration). Once the carbonation thickness has exceeded the coupled volume limit, the capacitive technique designates the concrete as homogeneous and shows stable values. These results indicate that, in practice, GE electrodes remain sensitive until roughly 20 mm for carbonation detection, i.e. much less than reported in previous studies for water content detection [Fares *et al.*, 2016].

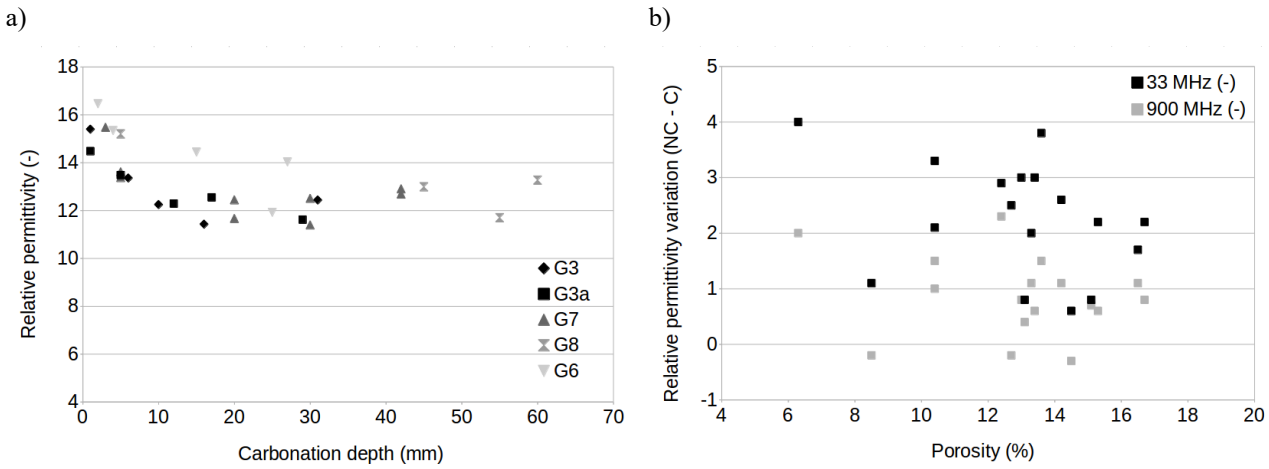


Fig. 8: Relative permittivity vs. carbonation depth during the carbonation process obtained by: a) capacitive technique, b) GPR

For the GPR results, the measurements display a slight decrease in evolution vs. carbonation depth (Fig. 7b), which is more visible over the first 20 millimeters. The underlying interpretation remains quite complex as several phenomena are interacting. The direct wave, whose maximum amplitude has peaked, corresponds to the sum of the direct wave in the medium, the faint direct air wave (as the antennas are shielded) and a possible guided wave propagating in the carbonated layer.

Concerning the Epsilon project, the deduced relative permittivity values, as obtained from EM cell measurements using Jonscher's model fitting at 33 and 900 MHz, are presented in Table 6. These results are rather similar to those from the ANR-SENSO project (Table 5), by showing decreases in relative permittivity with carbonation that are more pronounced at low frequencies than at the GPR frequency.

Moreover, capacitive measurements could be performed, following the project, on carbonated slabs (B samples) after saturation. The limitation with this method lies in the fact that the capacitive system was not available during the Epsilon project, in which concrete slabs (A samples) were not subjected to natural carbonation. Once available, the natural carbonation had progressed and was therefore no longer negligible in the capacitive measurements, which then could no longer be carried out on non-carbonated mixes.

The capacitive results, as featured in Table 6, show good agreement with the results obtained from the EM cell at the same frequency.

**Table 6: Variation in relative permittivity values at 33 and 900 MHz due to carbonation (Epsilon project)**

| Code | Capa_GE (-) | Jonscher's fitting 33 MHz (-) | Decrease 33 MHz | Jonscher's fitting at 900 MHz (-) | Decrease 900 MHz |
|---|---|---|---|---|---|
| C1_NC | | 14.7 | 2.0 | 11.9 | 1.1 |
| C1_C | 12.64 | 12.7 | | 10.8 | |
| C3_NC | | 9.2 | 1.1 | 7.1 | -0.2 |
| C3_C | 7.82 | 8.1 | | 7.3 | |
| B5A_NC | | 11.6 | 4.0 | 8.8 | 2.0 |
| B5B_C | 5.78 | 7.6 | | 6.8 | |
| B7A_NC | | 12.5 | 2.0 | 10.4 | 1.0 |
| B7B_C | 10.63 | 10.4 | | 9.4 | |
| B13A_NC | | 11.0 | 3.3 | 8.8 | 1.5 |
| B13B_C | 8.65 | 7.7 | | 7.3 | |
| B15A_NC | | 15.7 | 3.8 | 11.7 | 1.4 |
| B15B_C | 12.73 | 11.9 | | 10.2 | |
| B17A_NC | | 13.1 | 0.8 | 11.8 | 0.8 |
| B17B_C | 14.02 | 12.3 | | 11.1 | |
| B19A_NC | | 12.8 | 1.7 | 10.9 | 1.0 |
| B19B_C | 11.32 | 11.1 | | 9.8 | |
| B25A_NC | | 14.2 | 0.8 | 11.6 | 0.4 |
| B25B_C | 12.60 | 13.4 | | 11.2 | |
| B27A_NC | | 11.7 | 3.1 | 8.8 | 0.8 |
| B27B_C | 10.06 | 8.7 | | 8.0 | |
| B29A_NC | | 14.4 | 2.2 | 12.6 | 0.8 |
| B29B_C | 14.02 | 12.2 | | 11.8 | |
| B31A_NC | | 13.3 | 0.5 | 11.5 | -0.2 |
| B31B_C | 15.34 | 12.7 | | 11.8 | |

## 4.3 Comparison with the EM results

Figure 9a compiles all EM results, in focusing on the relative permittivity of saturated carbonated mixes vs. porosity. The measurements performed at 33 MHz are depicted in black dots and those at 900 MHz in gray. Let's note an apparent linear increase with porosity, mainly due to an increase in the volumetric water content filling the pores. The variation in relative permittivity between non-carbonated and carbonated mixes is highlighted in Figure 9b. These variation values are roughly in the range of 2 at 33 MHz and 1 towards 900 MHz.

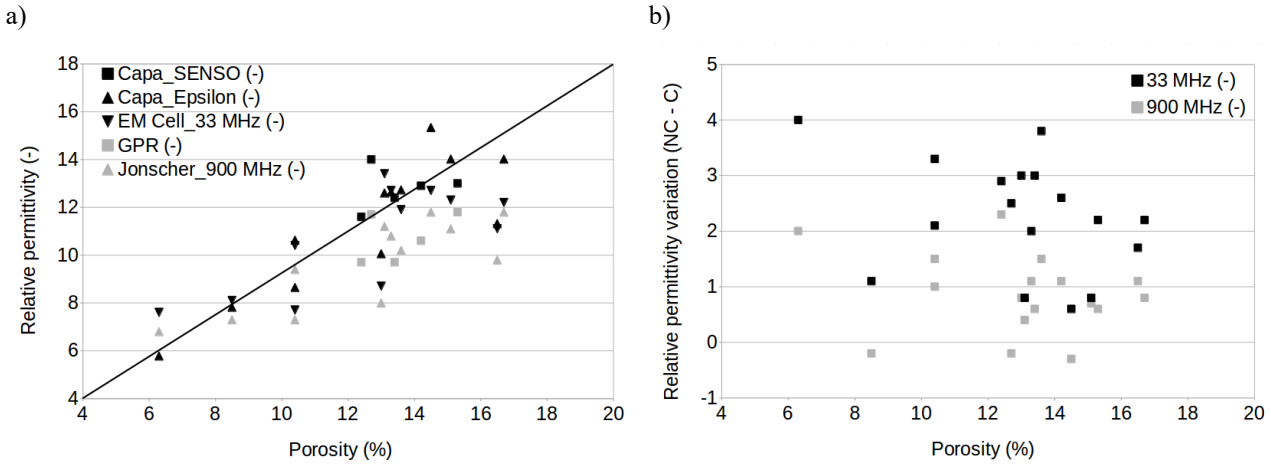


Fig. 9a) Relative permittivity vs. porosity obtained by capacitive and GPR techniques, and by EM cell measurements, as fitted by Jonscher's model on carbonated mixes; b) Variation of permittivity vs. carbonated porosity, derived by capacitive and GPR techniques, and by EM cell measurements fitted by Jonscher's model, compiled by frequency band.

While comparing non-carbonated and carbonated mixes, from the standpoint of EM NDT techniques, Figure 10 shows the level of permittivity shift at both ranges of frequency: a high one at 33 MHz and a low one at 900 MHz. The different presentations in Figures 9 and 10 are due to the fact that for the latest information, the separation step is based on aggregate type.

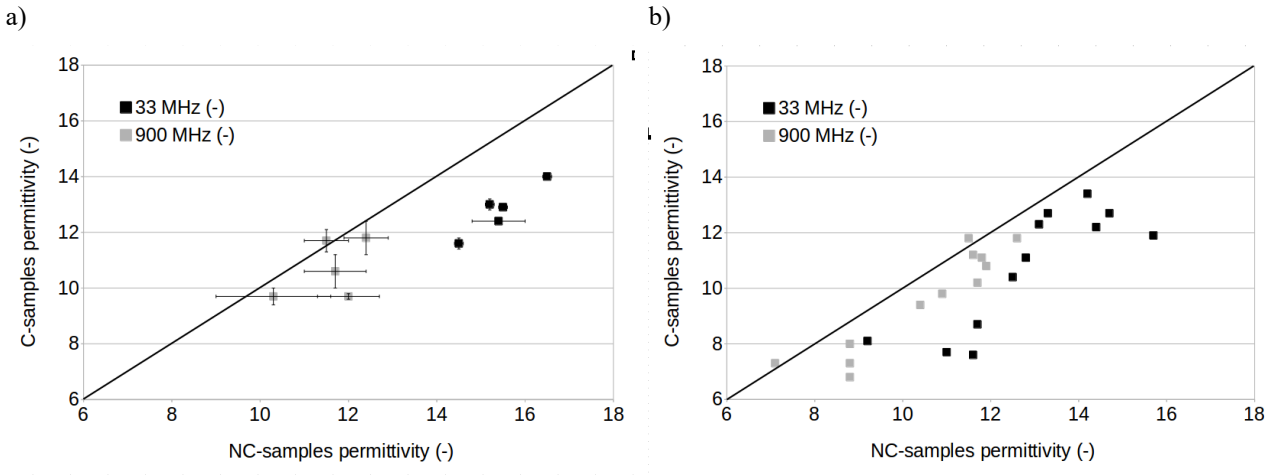


Fig. 10: Sensitivity to carbonation on capacitive techniques at 33 MHz and on GPR at 900 MHz using saturated concretes: a) ANR-SENSO project; b) Epsilon project

The decrease in the real part of permittivity, as determined by the GE capacitive technique, ranges from 2.2 to 3.0 (Table 5 and Fig. 5a) or from 0.8 to 4.0 (Table 6 and Fig. 5b). On the other hand, the decrease determined by GPR ranges between 0.6 and 2.2 or between 0.4 and 2.0.

These findings confirm that the results of both projects are in good agreement and moreover that the capacitive technique at 33 MHz is more sensitive than a GPR equipped with 1,500-MHz antennas to carbonation. This observation is in agreement with the higher sensitivity at low frequency revealed by the dispersion curves (Fig. 5). In addition, the uncertainty of capacitive measurements is much lower than that of GPR, as evidenced in Figures 7a and 10a.

## 5. Conclusion

The effect of carbonation on EM wave propagation and dispersion has been presented on (12+5) different saturated concretes, along with the capability of two electromagnetic non-destructive techniques, namely capacitive and GPR, to detect this pathology. Carbonation leads to a decrease in both the real and imaginary parts of permittivity. Wave attenuation is smaller and EM wave dispersion is reduced. This outcome can be attributed both to the porosity reduction that lowers the overall water content and to ionic changes in the pore solution. The pore distribution with fewer nano-pores and more micro-pores, which modifies tortuosity, could also exert an impact, mainly at low frequencies. The reason for choosing saturated mixes was twofold: maximize the variation in permittivity of non-carbonated and carbonated mixes, and remove any bias due to water content uncertainty in the mixes.

The results obtained from two national research projects are in agreement, indicating that carbonation induces a decrease in the range of 2 at 33 MHz and 1 towards 900 MHz for the permittivity of concretes. Moreover, saturated carbonated mixes display a general linear trend of permittivity vs. porosity due to the volumetric water content filling the pores.

Capacitive and GPR techniques could constitute useful tools for monitoring carbonation in concrete. Nevertheless, great care must be taken regarding the degree of saturation in the concrete samples since this parameter also heavily influences the EM results. For on-site ND structural evaluations, all durability indicators (porosity and degree of saturation) and degradation monitoring parameters (carbonation depth) must be assessed. Since all these indicators are capable of influencing EM NDT techniques, combining several complementary ND techniques might be required to perform independent evaluations.

## Acknowledgments

The authors are grateful to O. Coffec, J.L. Geffard and G. Gugole for their technical support. The Electricité de France (EDF) company and the French Ministry of Ecology (MTES) are also acknowledged for their financial support of the EPSILON research project. Also, the French National Research Agency (ANR) has generously sponsored the ANR-RGCU SENSO project.

## References

Adous, M., Queffelec, P. and Laguerre, L., 2006, Coaxial/cylindrical transition line for broadband permittivity measurement of civil engineering materials: Measurement Science and Technology, **177**, 2241–2246.

AFPC-AFREM, 1997, Méthodes recommandées pour la mesure des grandeurs associées à la durabilité,: in Journées techniques AFPC-AFREM sur la durabilité des bétons, Toulouse, France.

Alonso, C., Andrade, C. and González, J.A., 1988, Relation between resistivity and corrosion rate of reinforcements in carbonated mortar made with several cement types: Cement and Concr ete Research, **18**, 687-698.

Balayssac, J.P., Laurens, S., Arliguie, G., Breysse, D., Garnier, V., Dérobert, X. and Piwakowski, B., 2012, Description of the general outlines of the French project SENSO – Quality assessment and limits of different

NDT methods: Construction and Building Materials, **35**, 131-138.
Ballantyne, A.P, Alden, C.B., Miller, J.B., Tans, P.P. and White, J.W.C., 2012, Increase in observed net carbon dioxide uptake by land and oceans during the past 50 years: Nature, **488**, 70-72.
Benedetto A. and Pajewski L., 2015, Civil Engineering Applications of Ground Penetrating Radar, Eds: Benedetto A. and Pajewski, Springer, 371 pp.
De Larrard, T., Bastidas-Arteaga, E., Duprat, F. and Schoefs, F., 2014, Effects of climate variations and global warming on the durability of RC structures subjected to carbonation: Civil Engineering and Environmental Systems, **31,** 153–164.
Dérobert, X., Iaquinta, J., Klysz, G. and Balayssac, J.P., 2008, Use of capacitive and GPR techniques for non-destructive evaluation of cover concrete: Non Destructive Testing & Evaluation International, **41**, 44-52.
Dérobert, X. and Villain, G., 2017a, Development of a multi-linear quadratic experimental design for the EM characterization of concretes in the radar frequency-band: Construction and Building Materials, **136**, 237-245.
Dérobert, X. and Villain, G., 2017b, EM characterization of concretes, focused on water and chloride contents and carbonation, using multi-linear experimental designs in the radar frequency-band: Non Destructive Testing & Evaluation International, **92**, 187-198.
Dunster, A.M., 1989,. An investigation of the carbonation of cement paste using trimethylsilylation: Advances in Cement Research, **2**, 99-106.
Fares, M., Fargier, Y., Villain, G., Dérobert, X. and Palma-Lopes, S., 2016, Determining the permittivity profile inside reinforced concrete using capacitive probes: Non Destructive Testing & Evaluation International, **79**, 150-161.
Glass, G.K., Page, C.L. and Short, N.R., 1991, Factors affecting the corrosion rate of steel in carbonated mortars: Corrosion Science, **32**, 1283-1294.
Hernández-Paniagua, I.Y, Lowry, D., Clemitshaw, K.C, Fisher, R.E, France, J.L, Lanoisellé, M., Ramonet, M. and Nisbet, E. G., 2015, Diurnal, seasonal, and annual trends in atmospheric CO2 at southwest London during 2000–2012: Wind sector analysis and comparison with Mace Head, Ireland, Atmospheric Environment, **105**, 138-147.
Hong, S., Wiggenhauser, H., Helmerich, R., Dong, B., Dong, P., Xing, F., 2017, Long-term monitoring of reinforcement corrosion in concrete using ground penetrating radar: Corrosion Science, **114**, 123-132.
Hugenschmidt, J. and Loser, R., 2008, Detection of chlorides and moisture in concrete structures with GPR: Materials and Structures, **41**, 785-792.
Ihamouten, A., Chahine, K., Baltazart, V., Villain, G. and Dérobert, X., 2011, On the variants of frequency power law for the electromagnetic characterization of hydraulic concrete: IEEE Transaction on Instrumentation and Measurement, **60**, 3658-3668.
Jol H.M., 2009, Ground Penetrating Radar: Theory and Applications, ed.: Jol, Elsevier, 524 pp.
Kalogeropoulos, A., van der Kruk, J., Hugenschmidt, J., Bikowski, J. and Brühwiler, E., 2013, Full-waveform GPR inversion to assess chloride gradients in concrete: Non Destructive Testing & Evaluation International, **57**, 74-84.

Laurens, S., Balayssac, J.P., Rhazi, J. and Arliguie, G., 2002, Influence of concrete relative humidity on the amplitude of Ground-Penetrating radar (GPR) signal: Material and Structures, **35**, 198-203.

Papadakis, V. G, Vayenas, C. G. and Fardis, M N., 1991a, Fundamental modeling and experimental investigation of concrete carbonation: ACI Materials Journal, **88**, 363-373.

Papadakis, V. G, Vayenas, C. G. and Fardis, M N.,1991b, Experimental investigation and mathematical modelling of the concrete carbonation problem: Chemical Engineering Science, **46**, 1333-1338.

Parrott, L.J., 1987, A Review of Carbonation of Concrete: Cement and Concrete Association, 1987, 42 pp.

Peer, S., Case, J.T., Gallaher, E., Kurtis, K.E. and Zoughi, R., 2003, Microwave reflection and dielectric properties of mortar subjected to compression force and cyclically exposed to water and sodium chloride solution: IEEE Transaction on Instrumentation and Measurement, **52**, 111-118.

Persico R., 2014, Introduction to Ground Penetrating Radar – Inverse scattering and data processing, Ed: Persico, IEEE Press, 368 pp.

Ramonet, M., Delmotte, M. and Dacher, P., 2016, Un seuil record de CO2 franchi dans l'hémisphère Sud: ICOS-France, LSCE, CNRS, National Research Center, 2p. http:// www2.cnrs.fr/sites/communique/fichier/cp_amsterdam_vf_web.pdf

Robert, A., 1998, Dielectric permittivity of concrete between 50 Mhz and 1 Ghz and GPR measurements for building materials evaluation: Journal of Applied Geophysics, **40**, 89-94

Soustos, M.N., Bungey, J.H., Millard, S.G., Shaw, M.R. and Patterson, A., 2001, Dielectric properties of concrete and their influence on radar testing: Non Destructive Testing & Evaluation International, **34**, 419-25.

Tuutti, K., 1982, Corrosion of steel in Concrete: Research Report 4.82. Swedish Cement and Concrete Research Institute, Stockholm.

Utsi E., 2017, Ground penetrating radar – Theory and practice, BH Elsevier, 205 pp.

Villain, G., Ihamouten, A., du Plooy, R., Palma Lopes, S. and Dérobert, X., 2015, Use of electromagnetic nondestructive techniques for monitoring water and chloride ingress into concrete: Near Surface Geophysics, **13**, 299-309.

Villain, G. and Platret, G., 2006, Comparison of two experimental methods to determine carbonation profiles in concrete: ACI Materials Journal, **103**, 265-271.

Villain, G., Sbartaï, Z.M., Dérobert, X., Garnier, V. and Balayssac, J.P., 2012, Durability diagnosis of a concrete structure in a tidal zone by combining NDT methods: laboratory tests and case study.: Construction and Building Materials, **37**, 893–903.

Villain, G. and Thiéry, M., 2005, Impact of carbonation on microstructure and transport properties of concrete: in Proceedings of 10th Int. Conf. on Durability of Building Materials and Components, 8 pp.

Villain; G., Thiéry, M. and Platret, G., 2007, Measurement methods of carbonation profiles in concrete: thermogravimetry, chemical analysis and gammadensimetry: Cement and Concr ete Research, **7**, 1182–92.